Thermal blurring of event-by-event fluctuations generated by rapidity conversion

Yutaro Ohnishi,[1,*] Masakiyo Kitazawa,[1,2,†] and Masayuki Asakawa[1,‡]
[1]*Department of Physics, Osaka University, Toyonaka, Osaka 560-0043, Japan*
[2]*J-PARC Branch, KEK Theory Center, Institute of Particle and Nuclear Studies, KEK, 203-1, Shirakata, Tokai, Ibaraki 319-1106, Japan*
(Received 17 June 2016; revised manuscript received 26 August 2016; published 12 October 2016)

We study the effect of thermal blurring caused by the use of (momentum-space) rapidity as a proxy of coordinate-space rapidity in experimental measurements of conserved-charge fluctuations in relativistic heavy-ion collisions. In theoretical studies assuming statistical mechanics, calculated fluctuations are those in a spatial volume. Experiments, on the other hand, can measure fluctuations only in a momentum space in the final state. In a standard argument to compare experimental results for a momentum space with theoretical studies for a coordinate space, rapidities of particles are implicitly regarded as equivalent to their coordinate-space rapidity. We show that the relation of two fluctuations is significantly altered by the existence of the thermal motion, i.e., thermal blurring. We discuss that the thermal blurring can be regarded as a part of the diffusion process, and the effect can be understood by studying the rapidity window dependences of fluctuations. Centrality dependence of the thermal blurring effect is also discussed.

DOI: 10.1103/PhysRevC.94.044905

I. INTRODUCTION

In relativistic heavy-ion collisions, bulk fluctuations of conserved charges observed by event-by-event analyses are among unique hadronic observables which carry information on the thermal property of the medium in the early stage [1–4]; see a recent review, Ref. [5]. In particular, the non-Gaussianity of fluctuations characterized by higher order cumulants has acquired much attention recently [6–11]. Active measurements of fluctuations have been performed at Relativistic Heavy Ion Collider (RHIC) and the Large Hadron Collider (LHC) [12–17]. Measurements will also be carried out in future experiments, such as the beam-energy scan II (BES-II) program at RHIC [18] and future facilities, FAIR [19], NICA [20], and J-PARC [21]. Conserved-charge fluctuations can also be investigated in numerical experiments on the lattice [22,23]. The comparison between the real and virtual experiments by means of fluctuations will deepen our knowledge on statistical and dynamical aspects of relativistic heavy-ion collisions.

In the comparison of fluctuations measured by event-by-event analyses with those obtained by theoretical analyses, however, there is a difficulty associated with the phase space in which the fluctuations are defined [2–4]. On the theoretical side, including lattice QCD numerical simulations, the cumulants characterizing fluctuations are usually calculated on the basis of statistical mechanics [1–3,6–9,22]. The cumulants calculated in this formalism correspond to those in a finite *spatial volume* in equilibrium; the phase space is defined in *coordinate space* after integrating out the momentum [5]. On the other hand, in heavy-ion collisions experimental detectors cannot observe the position of particles in the medium. Instead, they can only measure the momentum of particles in the final state. Therefore, the phase-space defining fluctuations inevitably has to be chosen in *momentum space*.

The fluctuations in a momentum-phase space observed experimentally are usually regarded as a proxy of the one in a coordinate space as follows [2,3]. First, assuming the Bjorken space-time evolution, the (momentum-space) rapidity[1] y of a *fluid element* is equivalent to the coordinate-space rapidity $Y = \tanh^{-1}(z/t)$ of the fluid element because of boost invariance, where t and z are time and the longitudinal coordinate, respectively. Second, by assuming that the rapidities of *individual particles* in the fluid element is equivalent to the rapidity of the fluid element, rapidities of particles are identical with Y. Then, by measuring fluctuations in a rapidity window Δy after integrating out the transverse momentum, the phase space is regarded as the one in the coordinate space in a coordinate-space rapidity window $\Delta Y = \Delta y$, where transverse coordinates, x and y, are integrated out.

This argument, however, relies on two nontrivial assumptions: (1) validity of the Bjorken picture and (2) that the relative velocities of individual particles against the fluid element are negligible. Though the former may be justified for sufficiently high-energy collisions, the latter can be invalidated by thermal motion irrespective of collision energy. Because of the thermal motion, the correspondence between the two rapidities y and Y for individual particles becomes at most an approximate one. The measurement of fluctuation in Δy thus receives a blurring effect when the results are to be interpreted as fluctuations in ΔY. In this study, we call this effect *thermal blurring*, and investigate its effect on fluctuation observables quantitatively. We note that the existence of the thermal blurring effect has been pointed out in earlier studies [2–4,24]. The same problem is recently investigated in a slightly different context in Ref. [25]. The purpose of the present study is to investigate this effect on cumulants quantitatively. We discuss

*yonishi@kern.phys.sci.osaka-u.ac.jp
†kitazawa@phys.sci.osaka-u.ac.jp
‡yuki@phys.sci.osaka-u.ac.jp

[1]Pseudorapidity is often experimentally measured instead of rapidity because of the relative easiness of the measurement. In this paper, however, we consider rapidity because theoretically it has a preferable feature under Lorentz boost.

the centrality dependence of the thermal blurring effect and extend the argument to non-Gaussian fluctuations. The main results of this paper are presented in Ref. [26].

In this study, we estimate the thermal blurring effect by assuming that individual particles are emitted from the medium at kinetic freezeout. The thermal motion of individual particles at kinetic freeze-out is deduced from a simple blast-wave model for particle yields in $p_{\rm T}$ space. We show that the thermal blurring effect becomes more prominent as the rapidity window Δy becomes narrower, and at the maximal coverage of the rapidity window of STAR detector the observed fluctuations are significantly modified owing to this effect.

Because we consider the thermal blurring at kinetic freeze-out, our argument relates fluctuations observed experimentally to those in ΔY at kinetic freeze-out. When one wants to compare the experimental results with thermal fluctuations generated in a much earlier stage, one has to take account of the time evolution of fluctuations before kinetic freeze-out [10,24,28]. The time evolution is basically the diffusion process toward the equilibrium. In this paper we discuss that the thermal blurring can be regarded as a part of the diffusion process. One thus can use the mathematical results in Refs. [10,24,28] directly to understand the thermal blurring effects. We argue that the modification of fluctuations due to thermal blurring and diffusion can be experimentally understood by studying the rapidity window Δy dependences of the cumulants as discussed for the case of diffusion in Refs. [10,27,28]. The centrality dependence of net-electric charge fluctuation observed by ALICE Collaboration [14] is also discussed on the basis of this picture.

Throughout this paper, we assume the Bjorken space-time evolution. At lower energy collisions, this picture does not hold and our discussion would be significantly modified. We, however, do not consider such effects until Sec. VI.

This paper is organized as follows. In the next section we study thermal distribution of particles in rapidity space using a simple blast-wave model. In Sec. III, we then study the thermal blurring effects on cumulants. The formula of the cumulants are derived with two different methods in Secs. III A and III B. Numerical results are then shown in Secs. IV. In Sec. V, we then consider the effect of diffusion in the hadronic stage and show that the diffusion and blurring can be regarded as parts of a single diffusion process on the same footing. Section VI is devoted to discussions and a short summary.

II. THERMAL DISTRIBUTION IN RAPIDITY SPACE

In this section, we first discuss the magnitude of thermal blurring by studying the thermal distribution of particles in rapidity space at kinetic freeze-out on the basis of a blast-wave model.

In the Bjorken space-time evolution, the distribution of particle density in y space at coordinate-space rapidity Y, $n_Y(y)$ is related to the distribution at midrapidity $n(y)$ as

$$n_Y(y) = n(y - Y), \tag{1}$$

because of boost invariance. In what follows, we thus concentrate on $n(y)$.

The invariant momentum spectrum of particles crossing a surface element $d\Sigma_\mu$ is given by the Cooper-Frye formula [29],

$$E\frac{dN}{d^3\boldsymbol{p}} = d\Sigma \cdot pf(p\cdot u), \tag{2}$$

where $f(E)$ is the single-particle distribution in the rest frame and u_μ denotes the flow velocity. We assume the Boltzmann distribution for $f(E)$

$$f(E) \sim \exp\left[-\frac{E-\mu}{T}\right], \tag{3}$$

with the temperature T, chemical potential μ, and $E = \sqrt{m^2+\boldsymbol{p}^2}$ with m, denoting the mass of particles. The effect of quantum statistics on Eq. (3) is well suppressed for $T \ll m-\mu$. At kinetic freeze-out point with the temperature $T_{\rm kin}$, the effect of quantum statistics is negligible for all particles except for pions, on which the effect is at most about 10%.

In order to calculate the particle distribution $n(y)$ with Eq. (2), we employ the following simplified blast-wave model: We assume that the freeze-out with temperature $T_{\rm kin}$ and chemical potential $\mu_{\rm kin}$ takes place at a fixed proper time $\tau_{\rm kin}$ with a constant transverse velocity β.[2] The flow vector at midrapidity at $(t,x,y,z) = (t_{\rm kin},x,0,0)$ is given by $u_\mu = (\gamma,\beta\gamma,0,0)$ with $\gamma = (1-\beta^2)^{-1/2}$ while the surface vector $d\Sigma_\mu$ is proportional to $(1,0,0,0)$. Substituting them into Eq. (2), the momentum distribution of the emitted particles from the freeze-out surface at this point is given by

$$\frac{dN}{d^3\boldsymbol{p}} \sim \exp[-pu/T] = \exp[-\gamma(E+\beta p_x)/T], \tag{4}$$

where in the first proportionality we have used the fact that the μ dependence through $\exp(\mu/T)$ can be factored out. The particle spectrum emitted from freeze-out surface per unit rapidity y per unit transverse momentum $\boldsymbol{p}_{\rm T}$ is given by

$$\tilde{n}(\boldsymbol{p}_{\rm T},y) = \frac{dN}{d^3\boldsymbol{p}}\frac{dp_z}{dy}. \tag{5}$$

Using $dp_z = Edy$ and by integrating out the transverse momentum, we obtain the particle distribution per unit rapidity as

$$n(y) \sim \int dp_x dp_y E e^{-\gamma(E+\beta p_x)/T}, \tag{6}$$

where we have used the rotational invariance with regard to z axis, i.e., the longitudinal axis. The proportionality coefficient of $n(y)$ is determined so as to satisfy $\int dy n(y) = 1$. We note that Eq. (6) does not depend on μ. It is easily shown that $n(y)$ depends on m and T only through the combination $w = m/T$.

In Fig. 1 the distribution $n(y)$ is plotted for several values of $w = m/T$ and β. The figure shows that the distribution becomes narrower as w becomes larger. This dependence comes from the suppression of thermal motion at large w.

[2]In this model, therefore, possible dependence of $\tau_{\rm kin}$ on the position in transverse plane is neglected. The possible azimuthal angle dependence of β for peripheral collisions is not taken into account in this model, either.

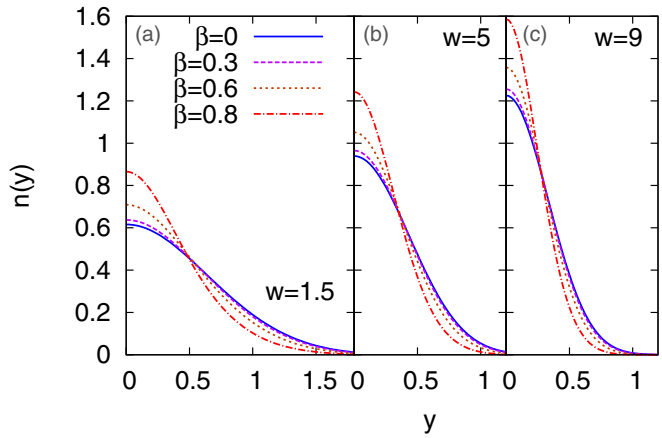

FIG. 1. Particle density per unit rapidity $n(y)$ for several values of $w = m/T$ and the transverse velocity β.

The figure also shows that the distribution becomes narrower for large β, which is a consequence of Lorentz effect; with the boost of a thermal system, the distribution is squeezed toward the direction of the boost.

In order to characterize the thermal distribution more quantitatively, we plot the width σ of $n(y)$ defined by

$$\sigma^2 = \int dy y^2 n(y), \tag{7}$$

as functions of w and β in the upper panels of Figs. 2 and 3, respectively. The blast wave fits for the p_T spectra at the LHC and top-RHIC energies for the most central collisions show that the freeze-out parameters are $T_{\rm kin} \simeq 100$ MeV and $\beta = 0.6$–0.7 [30]. With $T = T_{\rm kin}$, we thus have $w = m/T \simeq 1.5$ and 9 for pions and nucleons, respectively. Figures 2 and

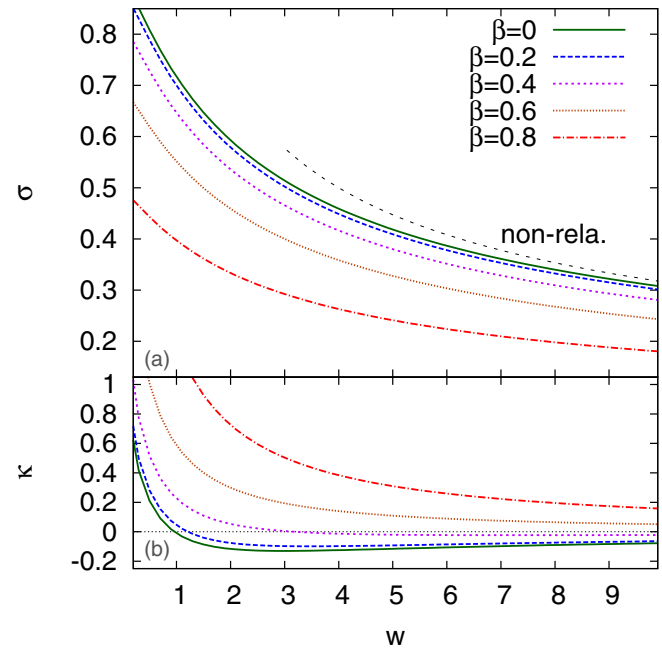

FIG. 2. Width σ and kurtosis κ of $n(y)$ as a function of $w = m/T$ for several values of transverse velocity β.

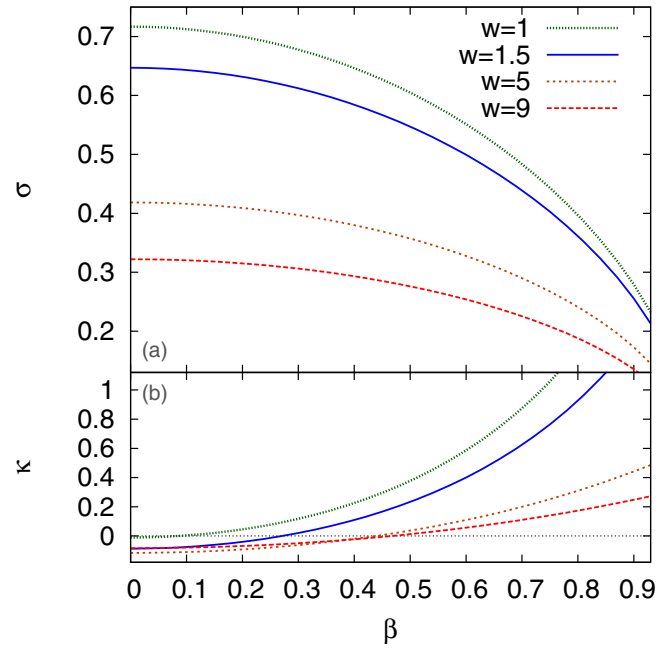

FIG. 3. Width σ and kurtosis κ of $n(y)$ as a function of transverse velocity β for several values of $w = m/T$.

3 show that the width of $n(y)$ for pions is $\sigma \simeq 0.5$ with the blast-wave parameters. This value is almost half the maximal rapidity window $\Delta y = 1.0$ at STAR [13]. Because the electric charge is dominantly carried by pions, this result suggests that the measurement of electric charge fluctuations with $\Delta y = 1.0$ [15] is strongly affected by thermal blurring. For nucleons, we have $\sigma \simeq 0.25$ with the same freeze-out parameters. The measurement of the baryon number cumulants [31] thus is less affected by thermal blurring than the electric charge, although the magnitude of σ in this case is not much suppressed compared to $\Delta y = 1.0$, either. In the next section, we analyze the thermal blurring effect more quantitatively by studying the cumulants directly.

Next, let us consider the deviation of $n(y)$ from Gauss distribution. Typical parameters to represent the deviation are the skewness S and kurtosis κ defined by [5]

$$S = \frac{1}{\sigma^3} \int dy y^3 n(y), \tag{8}$$

$$\kappa = \frac{1}{\sigma^4} \int dy y^4 n(y) - 3. \tag{9}$$

Because S and κ vanish for the Gauss distribution, their nonzero values characterize non-Gaussianity.[3] Since $n(y)$ is an even function, S always vanishes. In the lower panels of Figs. 2 and 3, the kurtosis of $n(y)$ is plotted for various parameters. Because the Maxwell-Boltzmann distribution in nonrelativistic gas is given by Gaussian, non-Gaussianity of $n(y)$ comes from relativistic effects. In fact, the figures show

[3]Here, we emphasize that S and κ defined here are the skewness and kurtosis *of* $n(y)$, respectively, and thus are different from those of event-by-event fluctuations of a conserved charge.

that the magnitude of κ becomes large for small w and large β, at which the relativistic effects become more prominent. For the parameters relevant to pions and nucleons at kinetic freeze-out, however, we have $|\kappa| < 0.5$, which indicates that the deviation from the Gauss distribution is not large. In Sec. IV we will show that the effect of non-Gaussianity of $n(y)$ on cumulants is indeed well suppressed.

In the nonrelativistic limit $w \to \infty$ and $\beta \to 0$, the distribution $n(y)$ approaches a Gauss distribution with the width $\sigma = 1/w$, which is shown by the dotted line in Fig. 2.

III. BLURRING EFFECT ON CUMULANTS

Next, we investigate the effects of thermal blurring on cumulants of a particle number $Q_{\Delta y}$ in a rapidity window Δy. To this end, in this section we first develop the formulation for the cumulants of $Q_{\Delta y}$ using two different methods, which give the same result. In Sec. III A, we first derive the result by only using the general properties of the cumulants and the binomial distribution function. We then obtain the same result in Sec. III B starting from a discretized formalism.

In this study, we investigate the thermal blurring effect focusing on the case that the density in Y space before thermal blurring is given by $\rho_Y(Y)$ and does not have event-by-event fluctuation. The density $\rho_y(y)$ in y space after thermal blurring has event-by-event fluctuations even in this case, and accordingly the cumulants $\langle (Q_{\Delta y})^n \rangle_c$ for $n \geqslant 2$ have nonzero values. Because $\langle (Q_{\Delta y})^n \rangle_c$ for $n \geqslant 2$ vanish without thermal blurring in this case, their nonzero values can be used as a measure of the magnitude of this effect. As we will discuss in Sec. III C, the fluctuations of $\rho_Y(Y)$ can straightforwardly be incorporated in this analysis following the treatment in Refs. [10,28].

A. Simple derivation

In order to describe the cumulants of $Q_{\Delta y}$, we first consider particles in an infinitesimal range dY in Y space before thermal blurring. The number of particles in dY is

$$N_{dY}(Y) = \rho_Y(Y) dY. \tag{10}$$

After thermal blurring, a particle in dY is found in the rapidity interval $-\Delta y/2 \leqslant y \leqslant \Delta y/2$ with probability

$$p_{\Delta y}(Y) = \int_{-\Delta y/2}^{\Delta y/2} dy n(y - Y). \tag{11}$$

See Fig. 4. Because of the nature of thermal blurring, this probability is to be regarded independent for individual particles. Therefore, the distribution of the particle number found in the rapidity interval Δy

$$q_{dY \to \Delta y}: \text{Number of particles which exist in } dY \text{ and are found in } \Delta y, \tag{12}$$

obeys the binomial distribution function,

$$B_{p,N}(m) = {}_N C_m p^m (1-p)^{N-m}, \tag{13}$$

with $p = p_{\Delta y}(Y)$ and $N = N_{dY}(Y)$. Using the fact that the nth order cumulant of Eq. (13) is given by [5]

$$\langle m^n \rangle_c = \xi_n(p) N, \tag{14}$$

we find that the cumulants of $q_{dY \to \Delta y}$ are given by

$$\begin{aligned} \langle (q_{dY \to \Delta y})^n \rangle_c &= \xi_n[p_{\Delta y}(Y)] N_{dY}(Y) \\ &= \xi_n[p_{\Delta y}(Y)] \rho_Y(Y) dY. \end{aligned} \tag{15}$$

The explicit forms of $\xi_n(p)$ up to the fourth order are

$$\begin{aligned} &\xi_1(p) = p, \xi_2(p) = p(1-p), \ \xi_3(p) = p(1-p)(1-2p), \\ &\xi_4(p) = p(1-p)(1-6p+6p^2). \end{aligned} \tag{16}$$

For the fifth and sixth orders, see Ref. [32].

The total number of particles $Q_{\Delta y}$ in Δy is obtained by summing up $q_{dY \to \Delta y}$ for all infinitesimal ranges dY as

$$Q_{\Delta y} = \sum_{\{dY\}} q_{dY \to \Delta y}. \tag{17}$$

To calculate the cumulants of $Q_{\Delta y}$, we note that the cumulants of the sum of uncorrelated stochastic variables are simply given by the sum of the cumulants [5]. Because $q_{dY \to \Delta y}$ should be uncorrelated for different dY bins, the cumulants of $Q_{\Delta y}$ are obtained as

$$\begin{aligned} \langle (Q_{\Delta y})^n \rangle_c &= \sum_{\{dY\}} \langle (q_{dY \to \Delta y})^n \rangle_c \\ &= \int dY \xi_n[p_{\Delta y}(Y)] \rho_Y(Y), \end{aligned} \tag{18}$$

where in the last equality we used Eq. (15) and replaced the sum with an integral. When the density $\rho_Y(Y)$ is uniform, $\rho_Y(Y) = \rho_0$, we have

$$\langle (Q_{\Delta y})^n \rangle_c = \rho_0 \int dY \xi_n[p_{\Delta y}(Y)]. \tag{19}$$

Next, let us see the behavior of Eq. (18) in the $\Delta y \to 0$ limit. In this limit, the probability $p_{\Delta y}(Y)$ should be suppressed proportionally to Δy irrespective of the value of Y. Because $\xi_n(p)$ in Eq. (14) satisfy $\xi_n(p) \to p$ for $p \to 0$ [5], we have

$$\xi_n[p_{\Delta y}(Y)] \to p_{\Delta y}(Y) \quad \text{for } \Delta y \to 0, \tag{20}$$

and the cumulants of $Q_{\Delta y}$ converge to a common value

$$\langle (Q_{\Delta y})^n \rangle_c = \int dY p_{\Delta y}(Y) \rho_Y(Y) = \langle Q_{\Delta y} \rangle, \tag{21}$$

for any $n \geqslant 1$. This result shows that $Q_{\Delta y}$ in this limit obeys a Poisson distribution [5].

For small but finite Δy, the probability $p_{\Delta y}(Y)$ may be expanded by a power series of Δy starting from the first

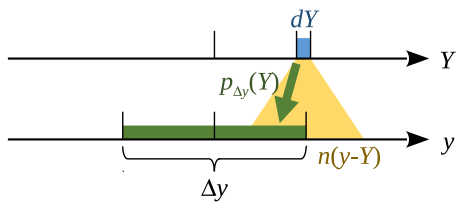

FIG. 4. Illustration of the rapidity window Δy and the probability $p_{\Delta y}(Y)$ in Eq. (11).

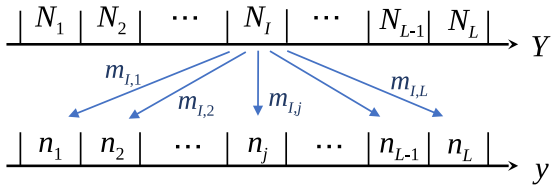

FIG. 5. Discrete system discussed in Sec. III B.

order. By substituting this expansion into Eq. (18) and using Eq. (14), one finds that the Δy dependence of $\langle (Q_{\Delta y})^n \rangle_{\rm c}$ is also expanded by a power series of Δy. The nth-order term in this expansion for $n \geqslant 2$ generally takes a nonzero value.

B. Derivation based on discretized formalism

Next, we derive Eq. (18) again but in a different way. In this subsection, we start from discretized coordinate spaces and take the continuum limit at the end.

We divide the coordinates Y and y into discrete cells with equal lengths δY and δy, respectively, as illustrated in Fig. 5. For simplicity, we further assume $\delta Y = \delta y$, though this is not essential in the following argument. For the moment, we assume that the total number of the cells L is finite in each space, although the final result does not depend on the finiteness of the number of cells. The distribution of particles in Y space is represented by the numbers of particles N_I in individual cells labeled by $I = 1,2,\ldots,L$. The distribution after thermal blurring in y space is also represented by the number of particles n_j in cells labeled by $j = 1,2,\ldots,L$.

As in the previous subsection, we consider the thermal blurring starting from a fixed distribution $\boldsymbol{N} = (N_1,\ldots,N_L)$ in Y space. Thermal blurring gives rise to fluctuation of the distribution $\boldsymbol{n} = (n_1,\ldots,n_L)$ in y space. We denote the probability distribution function of $\boldsymbol{n}$ by $P_y(\boldsymbol{n})$.

Owing to thermal blurring, a particle in a cell, say in the Ith cell, in Y space is distributed to various cells in y space. We denote the probability that the particle is found in jth cell in y space as

$$\begin{aligned} P_{I\to j}&\text{: the probability that a particle} \\ &\text{in the } I\text{th cell in } Y \text{ space is found} \\ &\text{in the } j\text{th cell in } y \text{ space.} \end{aligned} \tag{22}$$

Note that $\sum_j P_{I\to j} = 1$ has to be satisfied. Next, we consider the probability that N_I particles in the Ith cell are distributed in y space with $m_{I,j}$ particles in the jth cell as shown in Fig. 5. This probability is given by

$$p_I(\boldsymbol{m}_I; N_I) = f_{N_I}(\boldsymbol{m}_I; \boldsymbol{P}_I), \tag{23}$$

with $\boldsymbol{m}_I = (m_{I,1},\ldots,m_{I,L})$, $\boldsymbol{P}_I = (P_{I\to 1},\ldots,P_{I\to L})$, and the multinomial distribution function

$$f_{N_I}(\boldsymbol{m}_I; \boldsymbol{P}_I) = \frac{N_I!}{m_{I,1}!\ldots m_{I,L}!}\prod_j (P_{I\to j})^{m_{I,j}} \delta_{N_I, \sum_j m_{I,j}}, \tag{24}$$

where the Kronecker delta represents the conservation of particle number. The probability $P_y(\boldsymbol{n})$ is then given by the product of Eq. (23) after the sum over $m_{I,j}$ for all cells with a constraint $n_j = \sum_I m_{I,j}$ as

$$P_y(\boldsymbol{n}) = \prod_I \left[\sum_{\boldsymbol{m}_I} p_I(\boldsymbol{m}_I)\right] \prod_j \delta_{n_j, \sum_I m_{I,j}}. \tag{25}$$

To calculate the cumulants of $\boldsymbol{n}$, it is convenient to use generating functions [5]. The factorial moment generating function of Eq. (25) is calculated to be

$$\begin{aligned} G_{\rm f}(\boldsymbol{s}) &= \sum_{\boldsymbol{n}} \left[\left(\prod_j s_j^{n_j}\right) P_y(\boldsymbol{n})\right] \\ &= \prod_I \left[\sum_{\boldsymbol{m}_I} p_i(\boldsymbol{m}_I) \prod_j s_j^{m_{I,j}}\right] \\ &= \prod_I \left(\sum_j s_j P_{I\to j}\right)^{N_I}, \end{aligned} \tag{26}$$

with $\boldsymbol{s} = (s_1,\ldots,s_L)$. In the last step, we used Eqs. (23) and (24). The factorial cumulant generating function is then obtained as

$$K_{\rm f}(\boldsymbol{s}) = \ln G_{\rm f}(\boldsymbol{s}) = \sum_I N_I \ln\left(\sum_j s_j P_{I\to j}\right). \tag{27}$$

To take the continuum limit, $\delta Y \to 0$ and $\delta y \to 0$, of Eq. (27), we replace $N_i \to \rho_{\rm Y}(Y)\delta Y$ and $P_{I\to j} = n(y-Y)\delta y$. The sums over I and j in Eq. (27) then become integrals and one obtains the generating functional

$$K_{\rm f}[s(y)] = \int dY \rho_{\rm Y}(Y) \ln\left[\int dy s(y) n(y-Y)\right]. \tag{28}$$

The factorial cumulants of $Q_{\Delta y}$ are obtained by applying the operator

$$D_{\Delta y} = \int_{-\Delta y/2}^{\Delta y/2} dy' \frac{\delta}{\delta s(y')}, \tag{29}$$

to Eq. (28) and taking $s(y) = 1$ afterward as

$$\langle (Q_{\Delta y})^n \rangle_{\rm fc} = (D_{\Delta y})^n K_{\rm f}|_{s(y)=1}, \tag{30}$$

where the definition of the functional derivative $\delta/\delta s(y)$ is understood as the limit of the discretized notation. The cumulants of $Q_{\Delta y}$ are then obtained by using the relation between cumulants and factorial cumulants [5,28]. This manipulation leads to Eq. (18). We note that with $s(y) = 1$ the argument of logarithmic function in Eq. (28) becomes unity, $\int dy s(y) n(\eta - Y) = \int dy n(\eta - Y) = 1$, which makes the manipulation apparent.

C. Relation with diffusion master equation and initial fluctuation

Here, we note that Eq. (18) has the same form as the results of the cumulants $\langle (Q_{\Delta y})^n \rangle_{\rm c}$ obtained in the diffusion master equation (DME) [10,28] with fixed initial condition when $n(y)$ is replaced by a Gauss distribution with the

width $[2\int_0^t dt' D(t)]^{1/2}$, where $D(t)$ is the time (t)–dependent diffusion coefficient; see, Sec. 2.5 in Ref. [28]. This correspondence is reasonable, because in the DME individual particles composing the system behave independently, and the location of a particle at time t with a fixed initial position is distributed by a Gauss distribution owing to their random motion. Note that the Gaussianity of this distribution in the DME is consistent with the particle diffusion described by a diffusion equation [5,28].

The results in Eq. (18) are obtained for fixed initial density $\rho_Y(Y)$ without fluctuation. In Refs. [10,28], the solutions of the DME are obtained for initial conditions including fluctuations; see Sec. 2.7 in Ref. [28], for example. The derivation in these studies is applicable straightforwardly to the present problem, thermal blurring. When the fluctuation of $\rho_Y(Y)$ is taken into account, the result Eq. (18) for the first- and second-order cumulants is modified as

$$\langle Q_{\Delta y}\rangle_c = \int dY \langle \rho_Y(Y)\rangle_0 p_{\Delta y}(Y), \tag{31}$$

$$\langle (Q_{\Delta y})^2\rangle_c = \int dY \langle \rho_Y(Y)\rangle_0 \xi_2[p_{\Delta y}(Y)] + \int dY_1 dY_2 \langle \delta\rho_Y(Y_1)\delta\rho_Y(Y_2)\rangle_0 p_{\Delta y}(Y_1) p_{\Delta y}(Y_2), \tag{32}$$

where $\langle\cdot\rangle_0$ represents the expectation values taken for the distribution of $\rho_Y(Y)$ with $\delta\rho_Y(Y) = \rho_Y(Y) - \langle\rho_Y(Y)\rangle_0$. In Refs. [10,28], the result is also extended to describe the net-particle number, i.e., the difference of the particle and antiparticle numbers.

IV. NUMERICAL RESULTS

A. Rapidity window dependence

Next, we see the thermal blurring effect on $\langle (Q_{\Delta y})^n\rangle_c$ numerically. In this section, we consider the cumulants for homogeneous distribution in Y space, Eq. (19). In Fig. 6, we show the Δy dependences of the ratio of the cumulants normalized by the Poissonian value [28]

$$R_n(\Delta y) = \frac{\langle (Q_{\Delta y})^n\rangle_c}{\langle Q_{\Delta y}\rangle_c}, \tag{33}$$

for several values of w with $\beta = 0.6$ [30]. Because $R_n(\Delta y)$ should vanish without thermal blurring, their nonzero values represent a measure to see the magnitude of the thermal blurring effect. The figure shows that $R_n(\Delta y)$ for $n \geqslant 2$ becomes unity in the limit $\Delta y \to 0$. This result is consistent with Eq. (21), which states that the distribution of $Q_{\Delta y}$ becomes Poissonian in this limit. This limit can be regarded as the case that the information on the event-by-event fluctuations of $\rho_Y(Y)$ is completely lost owing to thermal blurring. On the other hand, $R_n(\Delta y)$ approaches zero for large Δy. This result shows that the thermal blurring effect is suppressed when $\Delta y \gg \sigma$ is satisfied. We note that the Δy dependence of the cumulants in Fig. 6 can be compared with the experimental results. For example, $R_2(\Delta y)$ is related to the D-measure D as $R_2(\Delta y) = D/4$ [4].

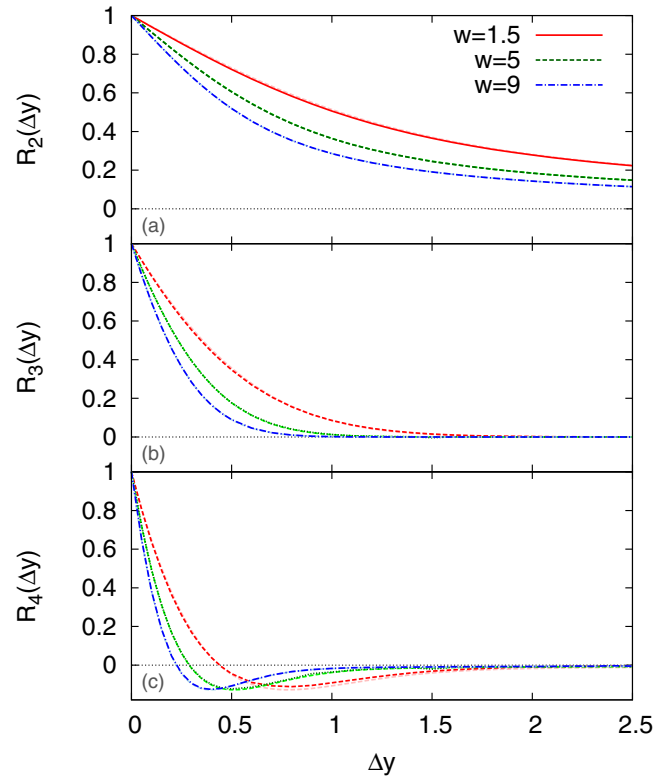

FIG. 6. Rapidity window dependences of the cumulants in normalization $R_n = \langle Q^n_{\Delta y}\rangle_c / \langle Q_{\Delta y}\rangle_c$ with vanishing initial condition for several values of $w = m/T$ with $\beta = 0.6$.

The maximal rapidity window of STAR detector is $\Delta y = 1.0$. The upper panel of Fig. 6 shows that the effect of thermal blurring is rather strong for the second-order cumulant with $\Delta y = 1.0$. For $w = 1.5$ corresponding to the electric charge fluctuation, we have $R_2(\Delta y) \simeq 0.5$. This result shows that the second-order cumulant of the electric charge fluctuation $\langle N_Q^2\rangle_c$ observed by STAR [15] receives about 50% modification due to thermal blurring. Because $\langle N_Q^2\rangle_c$ is modified, the ratio of the cumulants $\kappa\sigma^2 = \langle N_Q^4\rangle_c / \langle N_Q^2\rangle_c$ is also modified. The blurring effect is smaller at the maximal rapidity window of the ALICE detector $\Delta y = 1.6$ [14] or for $w = 9$ corresponding to net-baryon number cumulants. Even for these cases, however, $R_2(\Delta y)$ is larger than 0.25, which indicates that the thermal blurring effect is not well suppressed. The middle and lower panels of Fig. 6 show the results for the third- and fourth-order cumulants, $R_3(\Delta y)$ and $R_4(\Delta y)$. These panels suggest that the thermal blurring effect is more suppressed for higher order, but is not negligible for $\Delta y = 1.0$. In particular, the sign of the fourth-order cumulant can become negative owing to this effect.

From the results in Fig. 6, it is interesting to analyze the Δy dependences of the cumulants experimentally and compare with these results. In particular, the simultaneous analysis of the second-, third-, and fourth-order cumulants for electric charge and baryon number cumulants would enable us to confirm the validity of the picture on thermal blurring and to investigate its magnitude. We also note that the wider rapidity

coverage is desirable for the analysis of Δy dependences. The extension of STAR detector to cover wider Δy [18] thus will be quite effective for these analyses.

In order to see the effect of non-Gaussianity of $n(y)$ on our results, we calculate $\langle (Q_{\Delta y})^n \rangle_c$ by replacing $n(y)$ with a Gauss function with the width in Eq. (7). The results are shown by the lines with light colors in Fig. 6. The difference of these results from those with $n(y)$, however, is small and almost invisible in the figure except for $\langle (Q_{\Delta y})^4 \rangle_c$ with $w = 1.5$ having a small deviation. This result shows that one can safely replace $n(y)$ with a Gauss function in the study of $\langle (Q_{\Delta y})^n \rangle_c$ up to the fourth order. From the discussion in Sec. III C, this result also suggests that the thermal blurring effect can be described by the same manner as those developed in Refs. [10,28].

The result in Fig. 6 is obtained for the fixed initial density $\rho_Y(Y)$ without event-by-event fluctuation. When the event-by-event fluctuations of $\rho_Y(Y)$ are included, the Δy dependence of $R_n(\Delta y)$ is modified depending on parameters specifying the fluctuations of $\rho_Y(Y)$. Because this analysis is essentially the same as those addressed in Refs. [10,28], in the present study we just refer to Figs. 2 and 3 in Ref. [10] and Figs. 4–8 in Ref. [28], which show these results. An important remark on these results is that with the inclusion of the event-by-event fluctuations of $\rho_Y(Y)$, the thermal blurring effects on $R_3(\Delta y)$ and $R_4(\Delta y)$ can be enhanced significantly compared with the results in Fig. 6.

B. Centrality dependence

Next, we investigate the centrality dependence of the thermal blurring effect for the second-order cumulant. In the previous subsection we used parameters of the blast-wave model, $T_{\rm kin}$ and β, for the most central collisions. Because these parameters have centrality dependences [30], when one applies our results to noncentral collisions the freeze-out parameters have to be replaced with those corresponding to the centrality. The experimental results suggest that $T_{\rm kin}$ becomes larger while β becomes smaller from central to peripheral collisions [30]. The analysis in Sec. II suggests that both these dependences enhance the width of $n(y)$, and accordingly the thermal blurring effect.

In this subsection, we include the event-by-event fluctuations of $\rho_Y(Y)$ in the analysis in order to compare the results with experimental data, as it is known that $\rho_Y(Y)$ has such fluctuations in the early stage [2,3]. We assume that the correlation function of $\rho_Y(Y)$ has the form

$$\langle \delta\rho_Y(Y_1)\delta\rho_Y(Y_2)\rangle_0 = D_2\delta(Y_1 - Y_2)\langle \rho_Y(Y_1)\rangle_0. \quad (34)$$

Note that Eq. (34) is satisfied in the equilibrated medium [5], and would be well justified even near the QCD critical point [25]. Here, D_2 is a quantity which is proportional to susceptibility in the early stage [28] and is related to D-measure D [4] as $D_2 = D/4$.

The results in the previous sections without fluctuations of $\rho_Y(Y)$ are obtained with $D_2 = 0$, while in the hadron resonance gas model one has $D_2 \simeq 1$ [4,5]. By substituting Eq. (34) into Eq. (32) and assuming uniform average density $\langle \rho_Y(Y)\rangle_0 =$ ρ_0, one obtains [24]

$$\langle (Q_{\Delta y})^2 \rangle_c = \rho_0 \int dY \{\xi_2[p_{\Delta y}(Y)] + D_2[p_{\Delta y}(Y)]^2\}$$
$$= \rho_0 \left\{ 1 - (1 - D_2) \int dY [p_{\Delta y}(Y)]^2 \right\}. \quad (35)$$

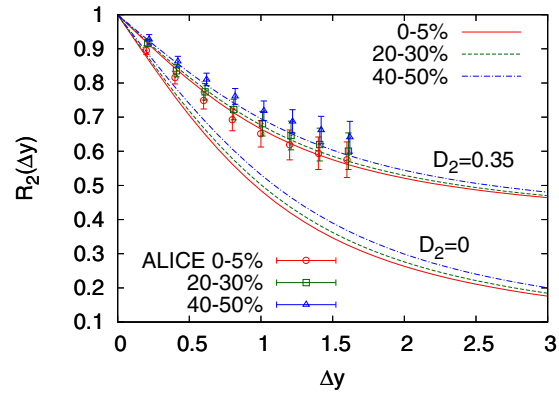

FIG. 7. Centrality dependence of the second-order cumulant of net-electric charge and the comparison with the experimental result by ALICE Collaboration [14].

In Fig. 7, we plot the Δy dependence of $R_2(\Delta y)$ with blast-wave parameters for centrality bins 0–5%, 20–30%, and 40–50% for ALICE experiment [30] for $D_2 = 0$ and 0.35. In the figure, we also show the D-measure observed by ALICE Collaboration with a translation $R_2(\Delta y) = D/4$ [4]. Here, we emphasize that D_2 is the D-measure in the initial condition, while $R_2(\Delta y)$ is the experimentally observed one with a rapidity window Δy, which takes a different value from D_2 owing to thermal blurring. The figure shows that the results for $D_2 = 0.35$ agrees with the experimental data within the error for all centrality bins. More accurate experimental data, however, are required to obtain a more quantitative conclusion. It, however, is notable that the qualitative centrality dependence observed in Ref. [30] is already well reproduced by thermal blurring and centrality independent D_2.

V. BLURRING AFTER DIFFUSION

Up to now, we have estimated the magnitude of thermal blurring, assuming that the particles are emitted from the hot medium at kinetic freeze-out time. In this argument, the distribution of $\rho_Y(Y)$ in Y space at *kinetic freeze-out* is related to the experimentally observed one after thermal blurring. On the other hand, the experimentally observed fluctuations are usually compared with thermal fluctuations in earlier stage, such as chemical freeze-out time or much earlier, in the literature. In this case, the modification of the event-by-event fluctuations in a rapidity window ΔY before kinetic freeze-out has to be taken into account besides the thermal blurring effect. We emphasize that the coordinate-space rapidities Y of individual particles and accordingly $\rho_Y(Y)$ in each event are changing before the kinetic freeze-out because of the nonzero velocity of individual particles along longitudinal direction [2,3,24].

If the motion of particles in Y space before kinetic freeze-out is well approximated by diffusion process, a particle at $Y = Y_0$ at some early proper time $\tau = \tau_0$ is distributed at kinetic freeze-out time $\tau = \tau_{\rm kin}$ in Y space by a Gauss distribution

$$P_{\rm drift}(Y_0 \to Y_{\rm kin}) \sim \exp\left(-\frac{(Y_{\rm kin} - Y_0)^2}{2d^2}\right), \qquad (36)$$

with the diffusion distance d. Note that d is related to the τ-dependent diffusion coefficients $D(\tau)$ and $D_{\rm Y}(\tau)$ in Cartesian and Bjorken coordinates, respectively, as [27,28]

$$d^2 = 2\int_{\tau_0}^{\tau_{\rm kin}} d\tau' \frac{D(\tau')}{\tau'^2} = 2\int_{\tau_0}^{\tau_{\rm kin}} d\tau' D_{\rm Y}(\tau'). \qquad (37)$$

After the diffusion in Y space, particles are observed at some rapidity y through thermal blurring. Then, the probability that a particle located at $Y = Y_0$ at $\tau = \tau_0$ is found at a rapidity y in the final state after thermal blurring, $P_{\rm D+B}(Y_0 \to y)$, is given by the convolution integral

$$P_{\rm D+B}(Y_0 \to y) = \int dY_{\rm kin} P_{\rm drift}(Y_0 \to Y_{\rm kin}) n(y - Y_{\rm kin}). \qquad (38)$$

Generally, the probability Eq. (36) of the diffusion motion for different particles can be correlated because the scattering of particles can give rise to such a correlation. We also note that the above argument does not take account of the possibility of pair creations and annihilations of particles. When one considers the baryon number for sufficiently large $\sqrt{s_{NN}}$, however, the correlation should be well suppressed because baryons in the hadronic medium almost exclusively interact with pions [31]. The chemical freeze-out picture also suggests that the pair creations and annihilations hardly occur after chemical freeze-out time. When these conditions are satisfied, the total effect due to the diffusion in Y space and thermal blurring can be described by simply replacing $n(y - Y)$ in Eq. (18) with $P_{\rm D+B}(Y_0 \to y)$ in Eq. (38). As discussed in Sec. IV A, the effect of non-Gaussianity of $n(y)$ is well suppressed. By approximating $n(y)$ by a Gauss distribution, $P_{\rm D+B}(Y_0 \to Y_{\rm kin})$ given by the convolution of two Gauss ones also becomes Gaussian. The total effect due to the diffusion and blurring then can be regarded as if it were from a single diffusion process, although the diffusion length, or the width of the Gauss distribution, includes both effects. In this picture, the results in Figs. 6 and 7 should be interpreted as the results with minimal diffusion lengths. We also note that the hadronic decays [34] give rise to diffusion of charges in rapidity space, and thus would be treated as a part of the diffusion and blurring to a good approximation. Finally, we note that the same conclusion on thermal blurring is also applicable to the interpretation of the balance function and correlation along rapidity direction [35,36] measured experimentally.

VI. SUMMARY

In this study, we investigated the thermal blurring effect, i.e., the effect arising from the use of rapidity y in substitution for the coordinate-space rapidity Y, on cumulants of conserved charges measured by the event-by-event analysis in relativistic heavy-ion collisions quantitatively. Our analysis suggests that the thermal blurring affects fluctuation observables significantly at the maximal rapidity coverage of STAR detector, $\Delta y = 1.0$, and not negligible even with $\Delta y = 1.6$ the maximal rapidity coverage of ALICE detector. When one compares the event-by-event fluctuation observed in these experiments with theoretical results obtained on the basis of statistical mechanics, therefore, the correction arising from the thermal blurring effect should be taken into account seriously.

Although we assumed the Bjorken space-time evolution throughout this paper, for low-energy collision this picture does not hold any more. For lower energy collisions the effect of global charge conservation will also show up [27,33]. These effects have to be considered seriously in the interpretation of experimentally observed fluctuations at BES-II energy region [18]. Throughout this study we also assumed that the transverse momentum is integrated out. In real experiments, however, the particles are observed in a finite transverse momentum acceptance. The understanding of the effect of the momentum cut [37] on fluctuations is another important issue. The comparison and estimate of the thermal blurring effects based on the dynamical models [11] are also interesting subjects for future study.

ACKNOWLEDGMENTS

The authors thank M. Sakaida for discussion. This work was supported in part by JSPS KAKENHI Grants No. 25800148 and No. 26400272.

[1] M. A. Stephanov, K. Rajagopal, and E. V. Shuryak, Phys. Rev. Lett. **81**, 4816 (1998).
[2] M. Asakawa, U. W. Heinz, and B. Müller, Phys. Rev. Lett. **85**, 2072 (2000).
[3] S. Jeon and V. Koch, Phys. Rev. Lett. **85**, 2076 (2000).
[4] V. Koch, arXiv:0810.2520 [nucl-th].
[5] M. Asakawa and M. Kitazawa, Prog. Part. Nucl. Phys. **90**, 299 (2016).
[6] S. Ejiri, F. Karsch, and K. Redlich, Phys. Lett. B **633**, 275 (2006).
[7] M. A. Stephanov, Phys. Rev. Lett. **102**, 032301 (2009).
[8] M. Asakawa, S. Ejiri, and M. Kitazawa, Phys. Rev. Lett. **103**, 262301 (2009).
[9] B. Friman, F. Karsch, K. Redlich, and V. Skokov, Eur. Phys. J. C **71**, 1694 (2011).
[10] M. Kitazawa, M. Asakawa, and H. Ono, Phys. Lett. B **728**, 386 (2014).
[11] C. Herold, M. Nahrgang, Y. Yan, and C. Kobdaj, Phys. Rev. C **93**, 021902 (2016).
[12] M. M. Aggarwal *et al.* (STAR Collaboration), Phys. Rev. Lett. **105**, 022302 (2010).
[13] L. Adamczyk *et al.* (STAR Collaboration), Phys. Rev. Lett. **112**, 032302 (2014).
[14] B. Abelev *et al.* (ALICE Collaboration), Phys. Rev. Lett. **110**, 152301 (2013).

[15] L. Adamczyk *et al.* (STAR Collaboration), Phys. Rev. Lett. **113**, 092301 (2014).
[16] J. T. Mitchell (PHENIX Collaboration), Nucl. Phys. A **904-905**, 903c (2013); E. O'Brien (PHENIX Collaboration), *ibid.* **904-905**, 264c (2013).
[17] X. Luo (STAR Collaboration), **PoS CPOD2014 (2015) 019**.
[18] STAR Collaboration' STAR Notes SN0598, 2014 (unpublished), https://drupal.star.bnl.gov/STAR/starnotes/public/sn0598.
[19] R. Rapp *et al.*, Lect. Notes Phys. **814**, 335 (2011).
[20] Design and construction of nuclotron-based ion collider facility (NICA) conceptual design report (unpublished), http://nica.jinr.ru/files/NICA_CDR.pdf.
[21] H. Sako *et al.* (J-PARC-HI Collaboration), White Paper for a Future J-PARC Heavy-Ion Program, 2016 (unpublished), http://asrc.jaea.go.jp/soshiki/gr/hadron/jparc-hi/.
[22] H. T. Ding, F. Karsch, and S. Mukherjee, Int. J. Mod. Phys. E **24**, 1530007 (2015).
[23] S. Borsanyi, **PoS LATTICE2015 (2015) 015**.
[24] E. V. Shuryak and M. A. Stephanov, Phys. Rev. C **63**, 064903 (2001).
[25] B. Ling and M. A. Stephanov, Phys. Rev. C **93**, 034915 (2016).
[26] M. Asakawa, *XXV International Conference on Ultrarelativistic Nucleus-Nucleus Collisions* (Quark Matter, Kobe, Japan, 2015).
[27] M. Sakaida, M. Asakawa, and M. Kitazawa, Phys. Rev. C **90**, 064911 (2014).
[28] M. Kitazawa, Nucl. Phys. A **942**, 65 (2015).
[29] F. Cooper and G. Frye, Phys. Rev. D **10**, 186 (1974).
[30] B. Abelev *et al.* (ALICE Collaboration), Phys. Rev. C **88**, 044910 (2013).
[31] M. Kitazawa and M. Asakawa, Phys. Rev. C **85**, 021901 (2012); **86**, 024904 (2012); **86**, 069902(E) (2012).
[32] M. Kitazawa, Phys. Rev. C **93**, 044911 (2016).
[33] M. Bleicher, S. Jeon, and V. Koch, Phys. Rev. C **62**, 061902 (2000).
[34] M. Nahrgang, M. Bluhm, P. Alba, R. Bellwied, and C. Ratti, Eur. Phys. J. C **75**, 573 (2015).
[35] S. Pratt, Phys. Rev. Lett. **108**, 212301 (2012).
[36] S. Gavin, G. Moschelli, and C. Zin, Phys. Rev. C **94**, 024921 (2016).
[37] F. Karsch, K. Morita, and K. Redlich, Phys. Rev. C **93**, 034907 (2016).